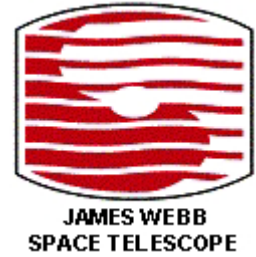


STSci-JWST-R-2002-0004

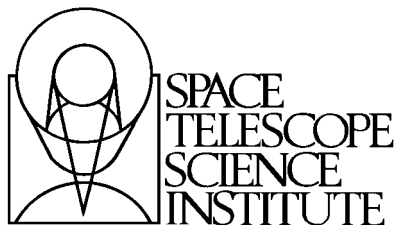


Space Telescope Science Institute  
James Webb Space Telescope Mission

---

## Comparison of Super-Sky and Self-Calibration Flat Fields for Simulated Mid-Infrared JWST Images

9 December, 2002  
Issue A



## REVISION HISTORY

ISSUE	DESCRIPTION	DATE
A	Initial Release	9-Dec-02

James Webb Space Telescope Mission

Comparison of Super-Sky and Self-Calibration Flat Fields  
for Simulated Mid-Infrared JWST Images

December 9, 2002

PREPARED BY:	<u>Stefano Casertano</u> NAME	<u>Instruments</u> ORG.
	_____ SIGNATURE	_____ DATE
	<u>Sherie T. Holfeltz</u> NAME	<u>Instruments</u> ORG.
	_____ SIGNATURE	_____ DATE

APPROVED BY: \_\_\_\_\_  
SIGNATURE

\_\_\_\_\_  
NAME

\_\_\_\_\_  
TITLE

# Comparison of Super-Sky and Self-Calibration Flat Fields for Simulated Mid-Infrared JWST Images

---

S. Casertano and S. T. Holfeltz  
December 9, 2002

---

## ABSTRACT

*The efficacy of two different flat-field calibration methods for JWST are considered. Flat fields obtained by the co-addition of sky flats and those obtained via self-calibration are quantitatively compared. Both methods can produce flat fields with an accuracy of a few parts in  $10^5$  that satisfy the JWST science requirements, as long as the instrumental response and background properties remain constant over several observing programs. The self-calibration method is quantitatively better, and is potentially more robust with respect to long-term changes in detector properties. The simpler super-sky flat method is probably preferable if instrumental and detector properties remain stable at the required level of accuracy.*

---

## Introduction

One of the scientific challenges that JWST must overcome to achieve its primary goals is the detection and measurement of small, faint sources at levels that approach  $10^{-4}$  of the sky brightness. As described in Casertano (2001), meeting this goal will most likely require the ability to subtract the background contribution, and determine the variation of the detector response function, or flat field, with accuracy of a few parts in  $10^5$  on scales ranging from the single pixel to the full field of view. The present report discusses and compares two techniques to correct for the background: super-sky flats and self-calibration.

### ***Super-sky flats***

Over the years, ground-based infrared observers have developed sophisticated schemes to extract the detector response function and subtract a potentially variable sky level from a sequence of images. A typical approach is to construct a synthetic sky by combining source-free regions of many different images, scaled to the same sky level. The underlying assumption is that the sky has the same shape in all images, although it may have a different overall level, and that sources can be rejected as outliers when comparing enough images taken at different pointings. The synthetic sky thus constructed is then scaled and subtracted from each image. If the underlying true sky is featureless, as expected under most circumstances, the sky image thus constructed is also a measurement of the detector response, and can be used as an inverse flat field - a *super-sky flat* - at least for sources that have the same color as the sky. In practice, in ground-based observations the assumption that the shape of the sky is constant is often only valid over a limited time span. Data processing procedures therefore include time filtering features, and consider only a window in time around each observation; the window is narrowed if there is evidence for pattern variations in the sky.

The JWST situation will likely be rather different: time variations in both sky level and shape will most likely be very small, except possibly for the background contribution from the telescope itself; therefore it should be possible to combine images from longer time series and forgo scaling. On the other hand, sources at a significant level may cover a larger area than in ground-based images, because of lower sky level, higher desired sensitivity, and longer integrations at each pointing. Therefore the ground-based techniques may need some modification for optimal application to JWST-like images, namely less sky scaling and time filtering, but more careful source filtering. In this report we test a simplified version of the ground-based algorithms, in which we solve for the flat field for the case of constant, flat sky.

### ***Self-calibration***

An alternate solution to determining and subtracting the sky in images containing a large contribution from sources has been suggested by Arendt, Fixsen and Moseley (Fixsen et al. 2000, Arendt et al. 2000), and goes under the name of self-calibration. In the self-calibration technique, no a priori assumption is made about the surface brightness distribution on the sky. On the contrary, the method allows the brightness of the observed scene to be an arbitrary function of position, only postulating that the brightness at each location be constant in time. Multiple images of the same area are taken while “dithering”, i.e., moving the telescope by an amount smaller than the field of view of the instrument. The method then solves for the detector sensitivity variation over the field of view, i.e., the flat field, by comparing the signal recovered when the same sky position is observed in different detector pixels. Once flat-fielded, all images are combined and the total luminosity is reconstructed; if necessary, the “sky” is subtracted as a constant value. The method can be

implemented in the form of a large but sparse least squares problem, and Arendt and Fixsen have made code available to the community to solve the problem. We carry out the self-calibration solution for the simulations presented here using an independent, iterative method developed by one of us (SC); our method is computationally somewhat less demanding than the Arendt and Fixsen solution, and produces essentially the same results.

### ***Comparison***

Super-sky flats and self-calibration are complementary approaches to the problem of correcting for the sky background. In principle, the self-calibration method has several advantages. First, the method can be used even if the image is filled with sources; there is no requirement that a large fraction of the sky be blank. Second, the method is more efficient in terms of signal-to-noise, since it uses all detector pixels, regardless of whether they contain a source or not; with the super-sky flat method, pixels with sources - which contain more flux than “empty” pixels - are excluded from the solution. Third, the flat field can be constructed from multiple images of the same small region of the sky, thus avoiding large slews that might introduce changes in the sky pattern. Finally, self-calibration is self-contained, in the sense that the sky can be flat-fielded and subtracted from the data obtained for a single program; this provides further protection against changes in the sky and flat field properties, and can simplify operational issues.

However, self-calibration may have some practical disadvantages in its implementation. The solution is computationally intensive, especially for the large-format images expected from NIRC*am*, and is more sensitive to image imperfections such as geometric distortion, subpixelation of sources, and variations in the point-spread function over the field of view. In operational terms, super-sky flats are best constructed from uncorrelated observations of independent regions of the sky, while self-calibration is suitable for observations dithered about a given sky position such that the same region of sky is imaged by several different detector pixels. As for the expected results, self-calibration yields tightly constrained calibrations for those pixels which have observed a common region of sky, while the relative calibration of pixels which have not imaged a common sky region are constrained indirectly by nearby pixels which have observed common sky regions; this can lead to non-trivial covariance between pixels that are not closely connected. Arendt et al. (2000) indicate that at least 20 well-spaced dithers are required for a self-calibration solution to be properly constrained.

The purpose of this investigation is to compare the performance of the super-sky flat and of the self-calibration methods, and to determine whether either method can deliver flat fields adequate to support the science goals of JWST. We use simulated images which take into account the expected distribution of sources at JWST sensitivity, as well as the expected properties of JWST instruments and detectors; we focus on the long-wavelength region, from 10 to 28  $\mu\text{m}$ , where the flat field requirements are the most demanding. For our exploratory purposes, our simulated images are an idealized representation of the sky,

with gain variable from pixel to pixel but constant in time and with noise that follows a well-defined model; we assume that all other imperfections, such as non-linearity, saturation, bias fluctuations, cosmic rays and so on are perfectly removed by the standard calibration. These simplifying assumptions allow us to compare the performance of the two methods under ideal conditions; more realistic simulations will be needed when more information is available on detector performance and instrument properties. Some estimates of the necessary calibration quality can be found in Casertano (2001). Since the primary goal of this study is to compare the two methods, we consider nearly ideal conditions, in which the only “imperfections” in the images are the flat field and a level of noise consistent with the detector characteristics of JWST. We use a standard “exposure time” of 25ks per pointing, representing a collection of deep observations suitable for the application of the super-sky flat fielding method. The same exposure time is used for individual pointings in the self-calibration method. The resulting observing pattern is not realistic, but it allows a direct comparison between the two methods. Further simulations should be carried out to represent realistic observing scenarios suitable for the application of each method.

Note that throughout this investigation, we equate “sky subtraction” with “flat fielding”. The reason is that in our simplified model, the true sky is always flat, and thus flat-fielding the data is necessary and sufficient for sky subtraction. In reality, these conditions may not be always applicable; possible examples include a color dependence of the flat field, combined with a systematic color difference between sky background and sources, and the presence of an internal background with structure that shifts with the pointing. Either method can be readily modified to handle a variety of more realistic conditions; in this exploratory study, we prefer to limit our considerations to the ideal case in order to obtain a more immediate comparison of the effectiveness of the two methods.

## **The Simulated Data**

The simulated data were generated by “observing” a simulated sky, generated so as to include a realistic distribution of sources and background, with an idealized detector with a fixed flat field pattern. For the self-calibration case, the detector was moved around on a single large sky image so as to cover a predefined dither pattern. Only integer pixel motions were considered. For the super-sky flat method, many different simulated sky images were generated and observed individually. The detector flat field included both large-scale variations of 20% peak-to-peak and pixel-to-pixel variations at the few percent level. We limited the detector size to 200x200 pixels; our results should scale with little change to larger detector size.

### ***Simulated Sky Data***

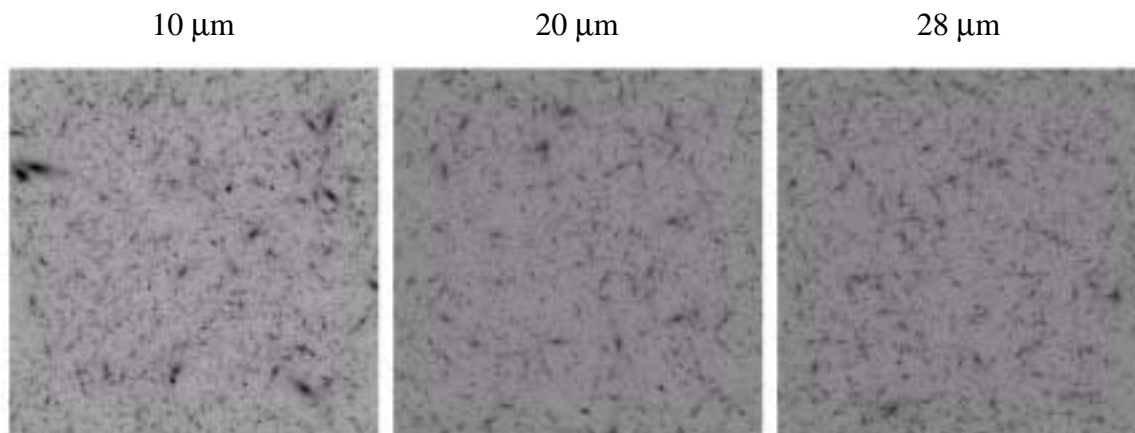
The simulated sky was created using code written by E. Morse in IDL. The simulations include a realistic distribution of galaxies, with size, luminosity, and spectral energy distri-

bution that roughly match available data. A realistic background, matching the prediction of the NGST Mission Simulator (NMS; Petro et al. 2001), is included. The appearance of individual galaxies is not especially realistic; they are represented by a smooth luminosity distribution, either a de Vaucouleurs law or an exponential. However, the simulated sky is expected to have approximately the correct combination of background and of source luminosity and size, which are the elements that should most affect the performance of the flat fielding methods. Individual sky images were generated at a pixel scale of  $0.3''$ , and were  $800 \times 800$  pixels each. Since realistic PSFs are not yet included in the sky simulation code, the sky images were convolved with an approximate PSF as part of the observing process described below. We considered three filters, centered at 10, 20, and  $28 \mu\text{m}$ , with a spectral resolution of 5; the filter characteristics are shown in Table 1, and typical simulated sky images in Figure 1.

**Table 1.** Simulated Filter Parameters (wavelengths in  $\mu\text{m}$ )

Peak Wavelength	Lower Wavelength	Upper Wavelength	Resolution $\lambda/\Delta\lambda$
10.	9.	11.	5
20.	18.	22.	5
28.	25.2	30.8	5

**Figure 1:** Simulated Sky Data for  $10 \mu\text{m}$ ,  $20 \mu\text{m}$ , and  $28 \mu\text{m}$



### *Simulated Flat Field*

The “true” flat field, which was kept constant throughout our calculations, is shown in Figure 2. It was designed to include a dome-like feature as well as 2-dimensional second order polynomial fluctuations and pixel to pixel variations. The large-scale features produce a  $\sim 20\%$  peak-to-peak variation in sensitivity, while the pixel to pixel variations are on the order of 2%-3%. The overall standard deviation is 0.04519; the mean is 1.000. The minimum and maximum values are, respectively, 0.8078 and 1.152.

**Figure 2:** “True” Flat Field

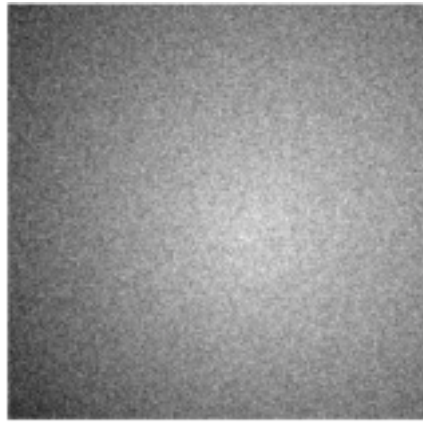


**Figure 3:** Example Dither Patterns and Exposure Maps for Random & Spiral Patterns

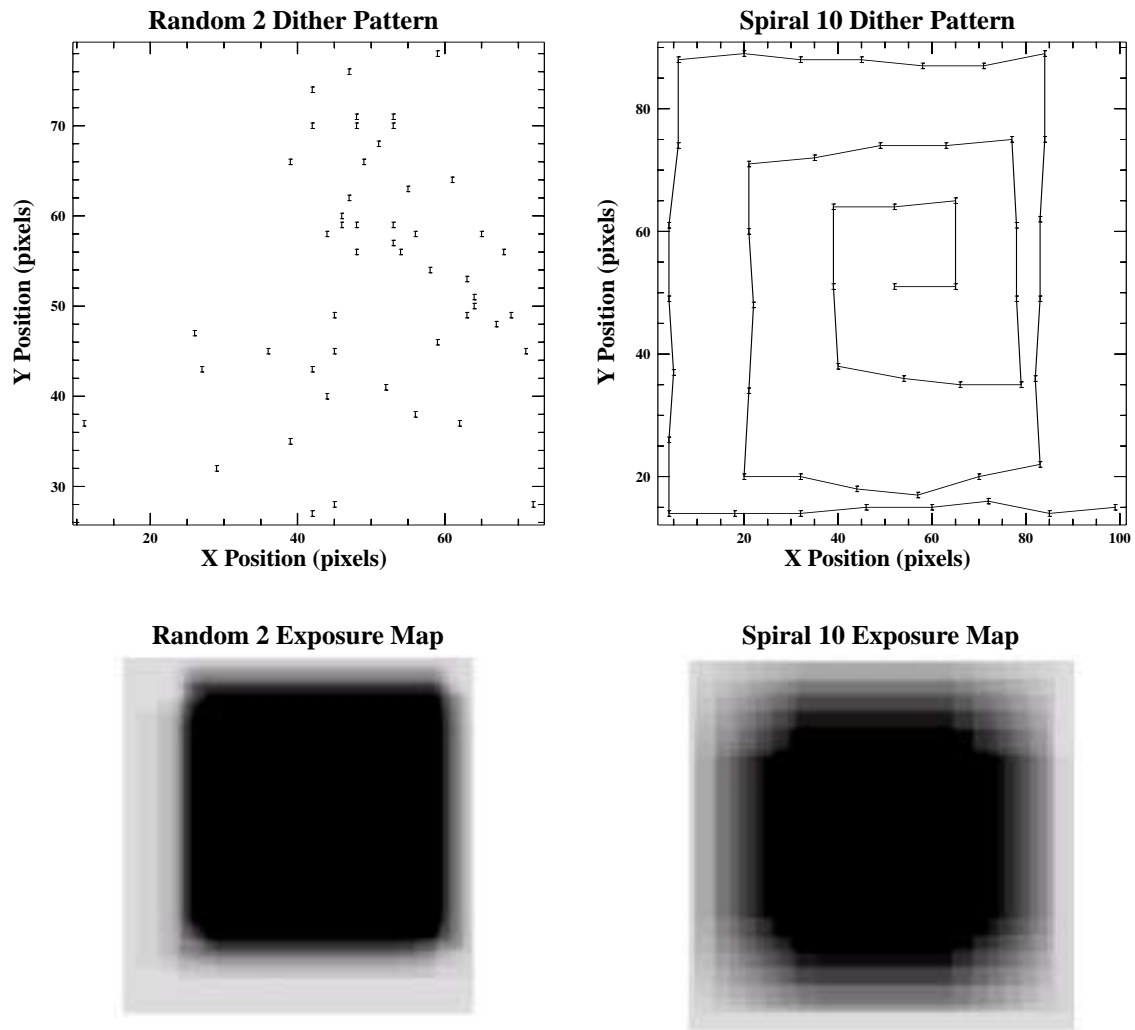


**Table 2.** Definition of Trial Patterns and Resulting Metrics for Simulation at 20  $\mu\text{m}$  with a PSF FWHM of 2 pixels.

Pattern	# Positions	$\Delta X$ (pixels)	$\Delta Y$ (pixels)	Flat Metric
Random1	100	50	50	6.0784801E-05
Random2	50	50	50	7.9921381E-05
Random3	75	50	50	6.3570900E-05
Random4	100	100	100	5.2579977E-05
Random5	50	100	100	7.4091753E-05
Random6	100	25	25	2.1322074E-03
Random7	50	25	25	1.1649994E-03
Random8	75	25	25	1.9252463E-03
Random9	100	50	50	6.1042330E-05
Random10	50	50	50	7.9772472E-05
Random11	100	100	100	5.2560594E-05
Random12	50	100	100	7.3643554E-05
Random13	75	100	100	5.9682625E-05
Random14	100	200	200	5.2634186E-05
Random15	50	200	200	7.4114891E-05
Spiral1	50	50	50	9.1519287E-05
Spiral2	50	75	75	3.9732648E-04
Spiral3	50	100	100	7.6984526E-03
Spiral4	100	25	25	5.1560855E-05
Spiral5	50	25	25	7.5295189E-05
Spiral6	50	25	25	7.6579192E-05
Spiral7	50	37	37	7.8633100E-05
Spiral8	50	50	50	8.0584621E-05
Spiral9	100	13	13	5.4542943E-05
Spiral10	50	13	13	7.2836272E-05
Spiral11	50	50	25	7.9391983E-05
Spiral12	50	75	50	5.5532256E-04
Spiral13	50	100	75	1.6295754E-03
Spiral14	100	25	12	5.1869767E-05
Spiral15	50	25	12	7.4161246E-05

***Simulated Sky Observations***

JWST will be diffraction limited at 2  $\mu\text{m}$  and is currently expected to have a primary mirror with a diameter of 6 m. The nominal full width at half maximum (FWHM) of the point spread function (PSF) at 2  $\mu\text{m}$  is thus 0.0839". Assuming a mid-infrared pixel size of 300 milliarcseconds, the FWHM expected at 10, 20 and 28  $\mu\text{m}$  is 1.4, 2.8, and 3.9 pixels, respectively. We convolved the simulated observations with a Gaussian of the appropriate FWHM. In order to limit the processing time, we used a reduced field of view of 200x200 pixels; the statistics of the results for the full field of view (1024x1024 pixels) of the mid-

infrared instrument (MIRI) should be essentially the same, with the only proviso that the dither pattern should be modified to cover the full scale of the detector in order to avoid low-level flat field features.

Several different dither patterns were simulated, including random patterns and spiral dithers. Spacecraft jitter was added to each dither position. Spiral dither pattern positions include additional small randomized offsets, a strategy found to yield substantially better fits. Only integer pixel shifts were considered: the dither positions were finally rounded to the nearest pixel. Example dither pattern positions and the resulting exposure map for typical random and spiral dither patterns are shown in Figure 3. For each position in a dither pattern, the true flat field was applied to the “observed” region of sky, followed by the addition of read noise and Poisson noise.

### **Self Calibration Flats**

The dithered observations described above were then used as self-calibration data to iteratively solve for the flat field and the sky, using software developed by one of us (SC). The iterative solution starts from a perfectly uniform flat field and constant sky. The current model is used to predict the observations; the difference between predicted and observed data is used to improve the current guesses, so that eventually the method converges to a final best-fit for both sky and flat field.

We used 15 Random and 15 Spiral patterns, with characteristics described in Table 2. For each pattern we give a name, the number of dither positions, the pattern scales  $\Delta X$  and  $\Delta Y$  in pixels, and a metric for the quality of the solution. For spiral patterns,  $\Delta X$  and  $\Delta Y$  denote the step size; for random patterns, the overall size of the region where the dithers are placed. The metric is simply the rms difference between the flat field estimated by the self-calibration method and the true flat field, for the 20  $\mu\text{m}$  case; the best cases have an rms below  $10^{-4}$ .

The performance of the method depends strongly on the pattern and scale of the dithers. Dither patterns with too much overlap, such as Random6, Random7, and Random8, do not yield enough pixel inter-relationships to allow a satisfactory solution. At the other extreme, insufficient overlap, such as in pattern Spiral13, also leads to failure. In addition, as mentioned above, strictly periodic step sizes also lead to insufficient data, as the same pixel relationships are repeated instead of expanded upon, leading to strong features in the solution. We have highlighted five patterns that yield a good solution free from systematic defects.

### **Super-Sky Flats**

For the super-sky flat simulation, we generated one hundred independent, unrelated sky patches, and observed each once with our simulated detector at 10, 20, and 28  $\mu\text{m}$ . We

convolved each observation with the appropriate Gaussian PSF, applied the detector flat field, and added the appropriate amount of Poisson and read noise.

The super-sky flats were constructed using iterative sigma clipping. First, an average (mean or median) image and a standard deviation image, calculated with respect to the average (mean or median), were determined from the observed data. Secondly, outliers beyond the  $5\text{-}\sigma$  threshold were iteratively clipped. The nearest 8 neighbors of the clipped data were also rejected. Finally, the average (mean or median) of the resulting unrejected data was taken as the super-sky flat field. The progression of iterative rejection and clipping is shown for one sky flat in Figure 4. In the figure, pixels whose values were beyond the rejection threshold are masked in grey; the resulting nearest neighbors which were clipped are shown in white.

**Table 3.** Effect of The Number of Valid Pixels on Superflat Flat Metric

# Sky Flats	Minimum # of Valid Sky Flat Pixels	Super-sky Flat Metric
3	0	0.0738003
4	0	0.0379486
5	1	0.000504900
6	1	0.000460179
7	2	0.000430757

The quality of the final flat field is measured with the same metric used for the self-calibration method, namely the rms difference between derived and true flat field. We track the properties of the resulting flat field as a function of the number of input images; not surprisingly, we find that the quality of the solution depends strongly on how many pixels have valid contributions from very few (or even zero) images. When the number of input images is small, several pixels may suffer from multiple source hits, and therefore have a poor estimate of the flat field. As the number of input images increases, this problem is alleviated quickly as long as the median is used. However, using the mean for source rejection and clipping results in a larger number of residual pixels affected by sources, and yields a poor solution even for a large number of images. As an example of these results, we give in Table 3 the number of sky flats, the minimum number of valid sky flat pixels per superflat pixel, and the resulting flat field metric for the first few  $28\ \mu\text{m}$  super-sky flats.

**Table 4.** Number of images required to obtain an acceptable flat field, i.e., for all pixels to have a valid value. Even 100 images were not enough at 10  $\mu\text{m}$  when using the mean.

Clipping	10 $\mu\text{m}$	20 $\mu\text{m}$	28 $\mu\text{m}$
Median	7	8	5
Mean	N/A	51	30

**Table 5.** Flat Field Metrics for Mean and Median Super-Sky Flats. The abnormally high value for Mean at 10  $\mu\text{m}$  is due to pixels without valid data.

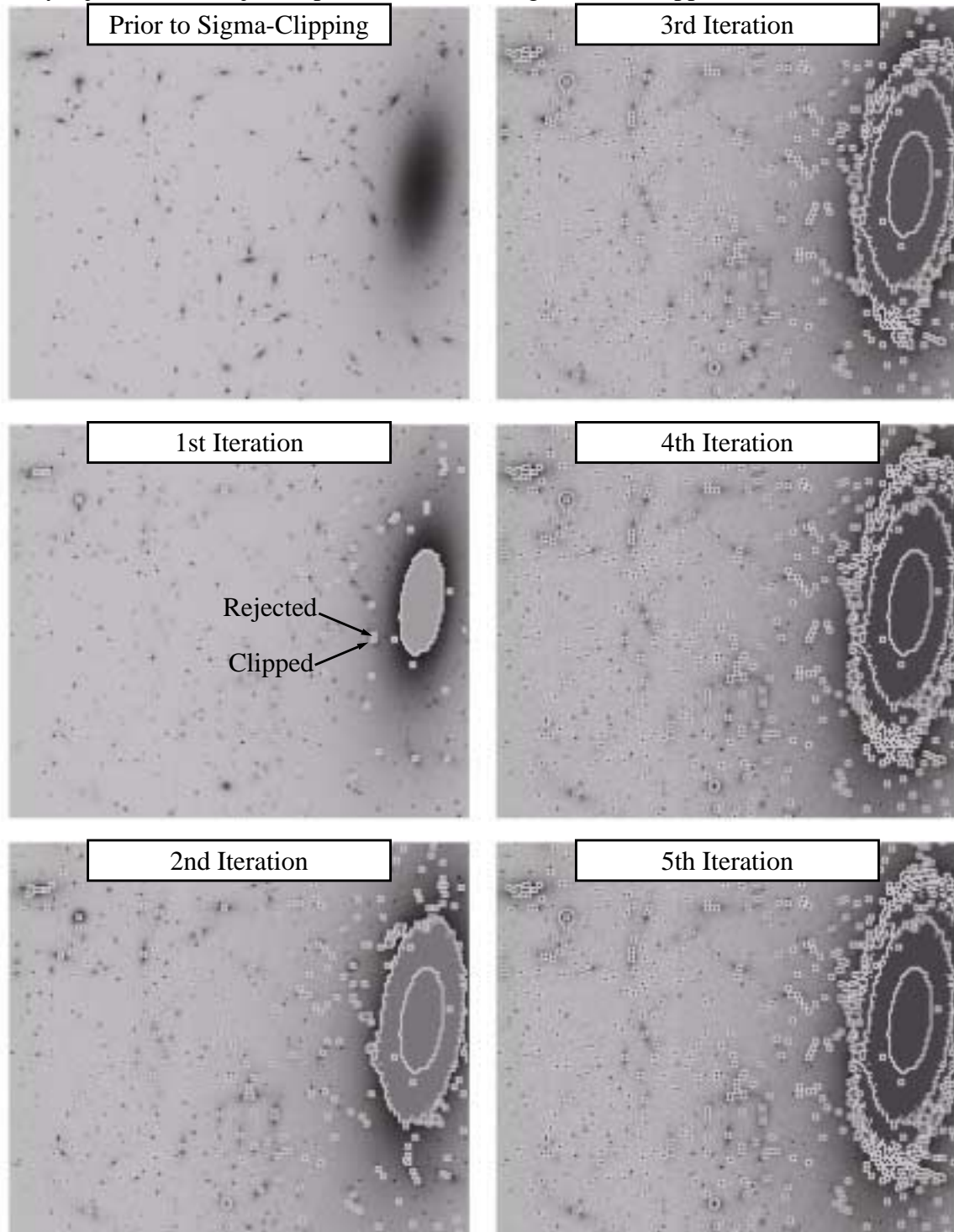
Wavelength ( $\mu\text{m}$ )	PSF FWHM (pixels)	Mean Flat Metric (n=100)	Median Flat Metric (n=100)
10	1.4	(1.53046E-02)	9.88215E-05
20	2.8	7.87431E-05	8.50129E-05
28	3.8	1.06971E-04	1.20936E-04

Simplistically, we can say that a super-sky flat field is “acceptable” if all detector pixels have a valid flat field value. This threshold is reached considerably sooner if the median is used instead of the mean in the sigma-clipping algorithm, as shown in Table 4. In fact, even 100 images are not sufficient for the mean to yield an acceptable flat field in the 10  $\mu\text{m}$  case. An illustration of the change in the number of valid sky flat pixels versus the number of sky flats is shown in Figure 5 for the 28  $\mu\text{m}$  super-sky flats.

The flat field metrics for the mean and median super-sky flats are shown in Table 5. The mean produces slightly better flats, due to the statistical advantage of the mean vs. the median, but fails to produce an acceptable flat field for the 10  $\mu\text{m}$  case, in which some pixels have no valid data even with 100 input images. Since the advantage of mean over median is otherwise small, its lack of robustness and need for a large number of images makes its use less desirable. In the following, we will restrict our consideration of super-sky flats to the use of the median.

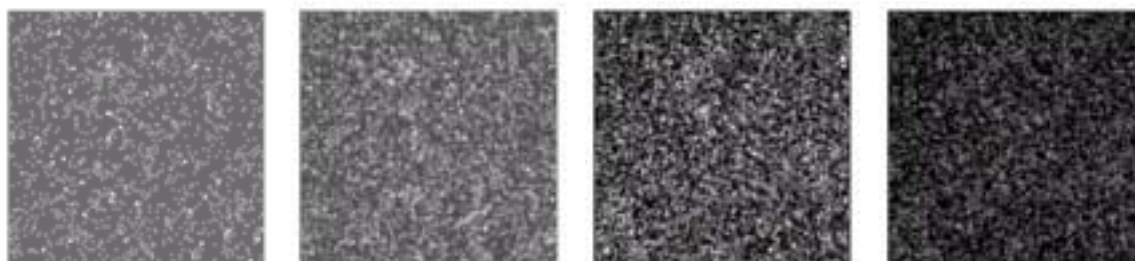
Table 6 shows how the flat field quality metric improves with the number of input images. The primary effect, as expected, is a scaling approximately as  $1/\sqrt{n}$ ; this can be seen more clearly in Figure 6, where the same data are presented in graphical form.

**Figure 4:** Progression of Iterative Rejection and Clipping. Pixels beyond  $5\text{-}\sigma$  are iteratively rejected and a rejected pixel's nearest 8 neighbors are clipped.



**Table 6.** Metrics for Median Super-Sky Flats as a Function of the Number of Images

# Sky Flats	10 $\mu\text{m}$	20 $\mu\text{m}$	28 $\mu\text{m}$
	1.4 Pixel FWHM	2.8 Pixel FWHM	3.9 Pixel FWHM
3	0.162887	0.106904	0.0738003
4	0.0759825	0.0441852	0.0379486
5	0.0248942	0.0150247	0.000504900
6	0.00845849	0.0123353	0.000460179
7	0.000298934	0.000293942	0.000430757
8	0.000279098	0.000275266	0.000403502
9	0.000261083	0.000259621	0.000384906
10	0.000252243	0.000247173	0.000364208
15	0.000215090	0.000203897	0.000299092
20	0.000186282	0.000183454	0.000260228
25	0.000173639	0.000164384	0.000234775
30	0.000158770	0.000151671	0.000214302
35	0.000146740	0.000140524	0.000199099
40	0.000137594	0.000131882	0.000186495
45	0.000132668	0.000125794	0.000176665
50	0.000126154	0.000119390	0.000168053
55	0.000121415	0.000115006	0.000160122
60	0.000116413	0.000109721	0.000153720
65	0.000115227	0.000105440	0.000147932
70	0.000112812	0.000101512	0.000142647
75	0.000110182	0.000097833	0.000137952
80	0.000108838	0.000094906	0.000134453
85	0.000106419	0.000092059	0.000131120
90	0.000103278	0.000089337	0.000127581
95	0.000100875	0.000087143	0.000124127
100	0.000098822	0.000085013	0.000120936

**Figure 5:** The Change in the Number of Valid Sky Flat Pixels as a Function of the Number  $n$  of Input Images.

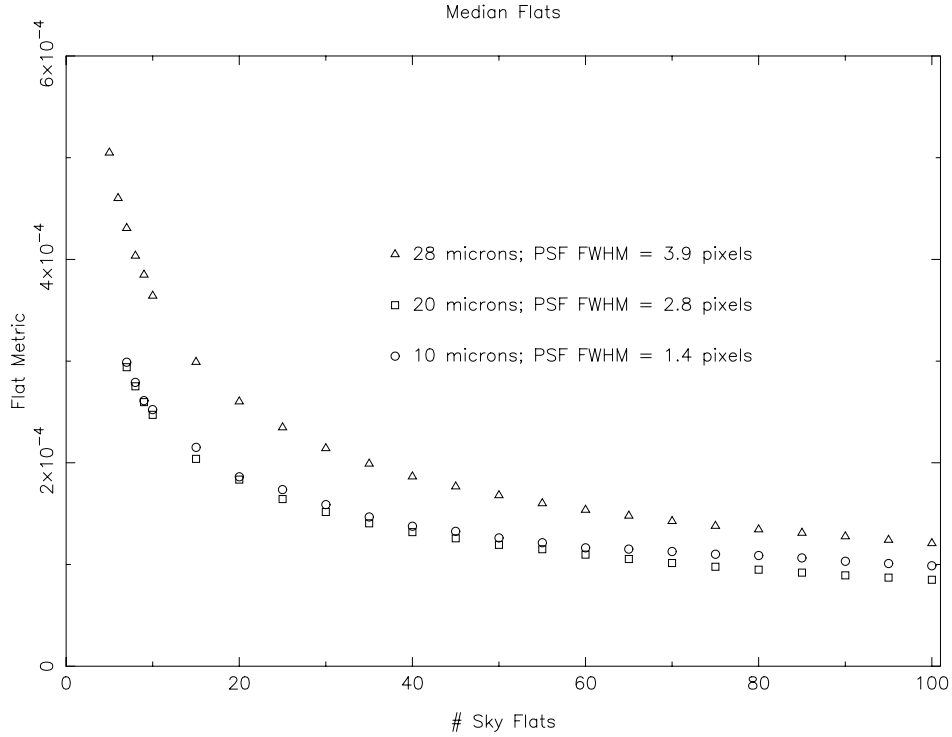
$n = 3$   
min. = 0  
mean = 2.654  
stddev = 0.5488

$n = 10$   
min. = 4  
mean = 8.867  
stddev = 1.001

$n = 50$   
min. = 34  
mean = 44.47  
stddev = 2.285

$n = 100$   
min. = 75  
mean = 88.96  
stddev = 3.392

**Figure 6:** Flat Field Metric for Super-Sky Flats vs. Number of Independent Images



### Comparison and Conclusions

The quantitative comparison of the self-calibration and super-sky flat methods is summarized in Table 7. Self-calibration with 100 well-dithered input images (the Spiral 4 and Spiral 9 cases) produces flat fields with rms deviations of approximately  $3.8 \times 10^{-5}$ ,  $5.3 \times 10^{-5}$ , and  $8.1 \times 10^{-5}$ , for 10, 20, and 28  $\mu\text{m}$ , respectively. The super-sky flats, using the median-based rejection and about 100 images, have rms deviations of  $9.9 \times 10^{-5}$ ,  $8.5 \times 10^{-5}$ , and  $1.2 \times 10^{-4}$ , respectively. Their performance is systematically worse, by a factor that decreases from 2.5 at 10  $\mu\text{m}$  to about 1.5 at 28  $\mu\text{m}$ . Thus, the self-calibration method is quantitatively somewhat superior to the super-sky flat fielding approach.

**Table 7.** Comparison of Flat Metrics for Self-Calibration & Super Sky Flat Fields

$\lambda$ ( $\mu$ )	Self-Calibration-Flat Metrics					Super-Sky-Flat Metric (n=100)
	Random 2 (n=50)	Random 10 (n=50)	Spiral 4 (n=100)	Spiral 9 (n=100)	Spiral 10 (n=50)	
10	5.7651618E-05	6.1108898E-05	3.7649927E-05	3.7293121E-05	5.3539381E-05	9.88215E-05
20	7.9921381E-05	7.9772472E-05	5.1560855E-05	5.4542943E-05	7.2836272E-05	8.50129E-05
28	1.1631714E-04	1.1913665E-04	8.1648090E-05	8.0660895E-05	1.1486391E-04	1.20936E-04

These results are only part of the story, however. In practice, most deep JWST observations will probably employ some dithering. When dithered observations are combined,

flat field imperfections will largely average out, and even the super-sky flat field will have sufficient quality to reach the theoretical limit of the observations, driven by photon and detector noise. Furthermore, if the instrument response is stable, both the super-sky flat field method and the self-calibration method can take advantage of observations from a large number of pointings, further reducing the flat field uncertainty. Under such circumstances, the simplicity of the super-sky flat field approach may make it more desirable compared with the more accurate, but more demanding self-calibration approach. On the other hand, should the instrument performance vary over time, self-calibration provides a unique way of determining an accurate flat field from each observing sequence.

A more realistic test of the flat field determination with JWST should include several items we have neglected here: 1) an appropriate combination of long and short observations; 2) a quantitative description of instrumental variations; 3) a proper description of the background, including both the flat sky and an internal background that moves with the telescope; and 4) a more detailed model of the observation process, including PSF variations, geometric distortion, and cosmic rays. Nonetheless, the simplified study presented here suffices to show that:

1. both self-calibration and super-sky flats can achieve the quality of flat fielding required by the JWST science program, as long as the instrumental response is constant to the required level over long time scales
2. self-calibration is preferable if the flat field and background must be determined from each observational program; super-sky flat fielding may be better if the detector response remains constant across several observing campaigns.

## References

- Arendt, R., Fixsen, R., and Moseley, H. 2000, *ApJ* 536, 500  
Casertano, S. 2001, *NGST Calibration Overview*, STScI-NGST-R-0014 A  
Fixsen, D., Arendt R., and Moseley, H. 2000, *ApJS* 128, 651  
Petro, L., et al. 2001, at <http://www.ngst.nasa.gov/public/configured/doc0472/rev03/DRM2.3.txt>